13

ETMM

ETMM13 Rhodes, Greece
15-17 September, 2021.

CONFERENCE PROCEEDINGS

TOWARDS LES OF BUBBLE-LADEN CHANNEL FLOWS: SUB-GRID SCALE CLOSURES FOR MOMENTUM ADVECTION

***E. Trautner*[1], *J. Hasslberger*[1], *T. Trummler*[1], *P. Cifani*[2], *R. Verstappen*[3] *and M. Klein*[1]**

[1] *Institute of Applied Mathematics and Scientific Computing*
Bundeswehr University Munich, Werner-Heisenberg-Weg 39, 85577 Neubiberg, Germany
[2] *Multiscale Modeling and Simulation, Faculty EEMCS*
University of Twente, P.O Box 217, 7500AE Enschede, The Netherlands
[3] *Bernoulli Institute for Mathematics, Computer Science and Artificial Intelligence*
University of Groningen, Nijenborgh 9, 9747AG Groningen, The Netherlands

elias.trautner@unibw.de

Abstract

This paper presents an *a-posteriori* assessment of different LES sub-grid scale closures for momentum advection in the context of bubble-laden channel flows. The numerical approach is based on the Volume-of-Fluid method in combination with the one-fluid formulation of the incompressible Navier-Stokes equations. To study the behavior of different sub-grid scale models, a turbulent bubble-laden downflow channel is simulated at a friction Reynolds number of $Re_\tau = 590$. The setup is chosen such that the bubbles are nearly spherical, but mildly wobbling. Both functional models of eddy viscosity type and scale similarity type models are used to close the sub-grid scale stresses. The results are compared to a direct numerical simulation of the same setup. It is found that the stream-wise volumetric flow rate depends strongly on the closure model as well as the grid resolution. While some models lead to an improvement compared to the LES without an explicit model, the comparably dissipative nature of the QUICK scheme prevents a clear assessment of some more advanced modeling strategies.

1 Introduction

Turbulent bubbly flow plays an important role in a large variety of technical applications, such as chemical reactors in the process industry or heat exchangers in power plants. Due to the increased computational power, Direct Numerical Simulation (DNS) has become feasible for reduced-complexity two-phase flow setups at limited Reynolds numbers. However, bubbly flows in industrial devices generally exhibit high Reynolds numbers, which limits the application of DNS to academic setups. Moreover, due to the presence of a second phase, the already wide range of scales of motion introduced by turbulence is possibly extended, preventing the usage of DNS for the design of most technical devices in the foreseeable future.

Consequently, Large Eddy Simulation (LES), which allows to resolve many physical processes to a large extent, while retaining the computational cost at an acceptable level, comes into focus. Compared to single-phase flow, multiphase flow LES is still in an early development stage. This is mostly due to the fact that additional unclosed terms are present in the respective governing equations. As *a-priori* analysis has shown, the dominant Sub-Grid Scale (SGS) contribution deserving the biggest attention stems from the convective term (Klein et al., 2019). In this paper, various models for this term are analysed based on *a-posteriori* LES and a comparison with results from a DNS of the setup. This is a first step towards a modeling strategy for bubbly flows, consisting of a set of LES closure terms that, due to the strong interaction, must be assessed in combination with a numerical method.

2 Governing equations and numerical method

The mathematical model implemented in the highly scalable open-source code "TBFsolver" (Cifani et al., 2018) is based on the one-fluid formulation of the incompressible Navier-Stokes equations. In the usual notation (density ρ, velocity components u_i, pressure p, dynamic viscosity μ, gravitational acceleration g_i, surface tension coefficient σ, interface normal n_i, interface curvature κ, interface Dirac function δ_S), the Favre-filtered LES equations (together with eq. (4)) read

$$\frac{\partial \widetilde{u}_i}{\partial x_i} = \tau_{\mathrm{div}u} \tag{1}$$

$$\begin{aligned}\frac{\partial \overline{\rho}\widetilde{u}_i}{\partial t} + \frac{\partial \overline{\rho}\widetilde{u}_i\widetilde{u}_j}{\partial x_j} &= -\frac{\partial \overline{p}}{\partial x_i} + \sigma \overline{n}_i \overline{\kappa}\overline{\delta}_S \\ &+ \frac{\partial}{\partial x_j}\left[\overline{\mu}\left(\frac{\partial \widetilde{u}_i}{\partial x_j} + \frac{\partial \widetilde{u}_j}{\partial x_i}\right)\right] + g_i\left(\overline{\rho} - \overline{\rho}_0\right) \\ &- \frac{\partial \tau_{\rho uu,ij}}{\partial x_j} + \frac{\partial \tau_{\mu S,ij}}{\partial x_j} + \tau_{nn,i}\end{aligned} \tag{2}$$

The average density in the domain is denoted as $\overline{\rho}_0$.

The convective SGS term, which is the scope of this paper, is represented by $\tau_{\rho uu,ij}$, while $\tau_{\mu S,ij}$, $\tau_{nn,i}$ and $\tau_{\mathrm{div}u}$ denote the diffusive SGS term, the SGS surface tension force and the residual in the divergence of the Favre-filtered velocity, respectively. Modeling the latter three is beyond the scope of this work. For the formulation implemented in the solver, the momentum equation (eq. (2)) has been divided by the density $\overline{\rho}$, so that the sub-grid stress tensor $\tau_{\rho uu,ij}$ can be expressed as $\tau_{uu,ij} = \widetilde{u_i u_j} - \widetilde{u}_i\,\widetilde{u}_j$.

The Continuum Surface Force approach is used to compute surface tension. In this context, the interface normal is defined as $\overline{n_i} = \nabla\overline{f}/\left|\nabla\overline{f}\right|$, where $\overline{f}$ is the filtered marker function for the local gas volume fraction in the context of the geometrical Volume-of-Fluid (VOF) method. The filtered interface curvature $\overline{\kappa} = \partial\overline{n_i}/\partial x_i$ is determined using a state-of-the-art height function method. The interface Dirac function $\overline{\delta}_S$ is numerically approximated as $\overline{\delta}_S = \left|\nabla\overline{f}\right|$. In each cell, the filtered density $\overline{\rho}$ and dynamic viscosity $\overline{\mu}$ are linearly interpolated from the liquid (l) and gas (g) phase material properties using the local gas volume fraction $\overline{f}$, i.e.,

$$\begin{aligned}\overline{\rho} &= \overline{f}\rho_g + \left(1-\overline{f}\right)\rho_l,\\ \overline{\mu} &= \overline{f}\mu_g + \left(1-\overline{f}\right)\mu_l.\end{aligned} \tag{3}$$

For the advection of the VOF marker function, a multiple-marker formulation (Coyajee & Boersma, 2009) is used to avoid numerical coalescence and handle bubble collisions. The single marker functions $b = 1, ..., N$ (with the total number of bubbles N) are advected (eq. (4)) using a geometrical interface reconstruction approach.

$$\frac{\partial\overline{f}_b}{\partial t} + \frac{\partial\widetilde{u}_j\overline{f}_b}{\partial x_j} = 0,\ \overline{f}_b = \begin{cases}1 & \text{for gas}\\ 0 & \text{for liquid}\end{cases} \tag{4}$$

Time integration is performed using a second-order Adams-Bashforth scheme. For stability reasons (Ketterl et al., 2019), the convective term is discretized using the third-order QUICK scheme, and central differences are used for the diffusive terms. The velocity components are arranged on a staggered grid. To allow the utilization of a fast Poisson solver (Dodd & Ferrante, 2014), the Poisson equation for pressure is transformed into a constant-coefficient formulation (Cifani, 2019).

3 Models for the convective SGS term

Models for the convective SGS term can be distinguished into functional and structural models. Functional models are mainly supposed to represent the forward energy cascade process. Two well known examples are the standard Smagorinsky model (eq. (5)) and the sigma model by Nicoud et al. (2011, eq. (6)), which both are of eddy viscosity type. The SGS stress tensor $\tau_{uu,ij} = \widetilde{u_i u_j} - \widetilde{u}_i\,\widetilde{u}_j$ is approximated using the concept of an eddy viscosity ν_t.

$$\begin{aligned}\tau_{uu,ij}^{\text{Smago}} &= -2\nu_t\widetilde{S}_{ij},\ \ \nu_t = (C_s\Delta)^2\left|\widetilde{S}_{ij}\right|\\ \left|\widetilde{S}_{ij}\right| &= \sqrt{2\widetilde{S}_{ij}\widetilde{S}_{ij}},\ \ C_s = 0.17\end{aligned} \tag{5}$$

In eq. (6), the singular values σ_i, ordered such that $\sigma_1 \geq \sigma_2 \geq \sigma_3$, are the square roots of the eigenvalues of G_{ij}.

$$\begin{aligned}\tau_{uu,ij}^{\text{Sigma}} &= -2\nu_t\widetilde{S}_{ij}\\ \nu_t &= (C_\sigma\Delta)^2\,\frac{\sigma_3\left(\sigma_1-\sigma_2\right)\left(\sigma_2-\sigma_3\right)}{\sigma_1^2}\\ G_{ij} &= \frac{\partial\widetilde{u}_k}{\partial x_i}\frac{\partial\widetilde{u}_k}{\partial x_j},\ \ C_\sigma = 1.35\end{aligned} \tag{6}$$

Here, $\widetilde{S}_{ij} = (1/2)(\partial\widetilde{u}_i/\partial x_j + \partial\widetilde{u}_j/\partial x_i)$ denotes the grid-scale strain rate.

In addition, a recently proposed dynamic modification of the Smagorinsky model by Hasslberger et al. (2021) is investigated. It is based on the coherent structure function $F_{CS} = Q/E$, which is compared on two different scales: implicitly filtered by the grid (F_{CS}) and explicitly filtered ($\widehat{F}_{CS}$) using the test filter by Anderson & Domaradzki (2012). In this context, Q is the second invariant of the grid-scale velocity gradient tensor, which is normalized by its magnitude E.

$$Q = -\frac{1}{2}\frac{\partial\widetilde{u}_j}{\partial x_i}\frac{\partial\widetilde{u}_i}{\partial x_j},\ \ E = \frac{1}{2}\frac{\partial\widetilde{u}_j}{\partial x_i}\frac{\partial\widetilde{u}_j}{\partial x_i} \tag{7}$$

The model is then given as

$$\tau_{uu,ij}^{\text{Sensor}} = \tau_{uu,ij}^{\text{Smago}}\left|\widehat{F}_{CS} - F_{CS}\right|^{3/2} C_{\text{Sensor}} \tag{8}$$

When used together with the QUICK scheme, the constant is set to $C_{\text{Sensor}} = 1/0.13$. This sensor-based modification has two main advantages: firstly, it can dynamically deactivate SGS dissipation if no sub-grid activity is present. Secondly, the exponent $3/2$ rectifies the incorrect near-wall scaling of the standard Smagorinsky model.

Structural models, on the other hand, are not restricted to the representation of the forward energy transfer, but instead aim to directly model the sub-grid tensor. While structural models generally reveal better performance in the context of *a-priori* analysis (Klein et al., 2019), they often become unstable when applied in *a-posteriori* LES. To further analyse this in the context of bubble-laden channel flow, several Scale Similarity Type (SST) models are investigated.

Using the tensor diffusivity model of Clark et al. (1979), the SGS stress tensor is calculated as

$$\tau_{uu,ij}^{\text{Clark}} = \frac{\Delta^2}{12}\frac{\partial\widetilde{u}_i}{\partial x_k}\frac{\partial\widetilde{u}_j}{\partial x_k}. \tag{9}$$

The scale similarity model of Liu et al. (1994) determines the tensor by applying an explicit secondary filter $\widehat{(\cdot)}$:

$$\tau_{uu,ij}^{\text{Liu}} = \widehat{\widetilde{u}_i\widetilde{u}_j} - \widehat{\widetilde{u}}_i\widehat{\widetilde{u}}_j. \tag{10}$$

Here, the secondary filter is chosen to be the same as for the previously explained sensor-based model.

In order to stabilize scale similarity type models, different regularization strategies have been proposed in an effort to prevent destabilization caused by backscatter. Klein et al. (2020) proposed a regularized, parameter free modeling strategy that can be applied to arbitrary structural models τ_{ij}^{SST}:

$$\tau_{uu,ij}^{\mathrm{KKK}} = \tau_{ij}^{\mathrm{SST}} - \max\left\{ \frac{\tau_{ab}^{\mathrm{SST}} \widetilde{S}_{ab}}{\widetilde{S}_{ab}\widetilde{S}_{ab}} \right\} \widetilde{S}_{ij}. \qquad (11)$$

In this work it is used to regularize Clark's model.

4 Flow configuration

The setup investigated in this work, as shown in Figure 1, is a vertical downflow (i.e., bubbles rising relative to the surrounding liquid) channel of size $L_x = 4H$, $L_y = 2H$ and $L_z = 2H$, where H denotes the channel half width. In the stream-wise (x) and the span-wise (z) directions, periodic boundary conditions are imposed, whereas the wall-normal y-direction is bounded by no-slip walls. The flow is driven downward by imposing a constant pressure gradient in x-direction, which is identical for all investigated setups and corresponds to a friction Reynolds number of $Re_\tau = (\sqrt{\tau_w/\rho_l}H)/\nu_l = 590$. Here, τ_w is the average wall shear stress, and ν_l denotes the liquid phase kinematic viscosity.

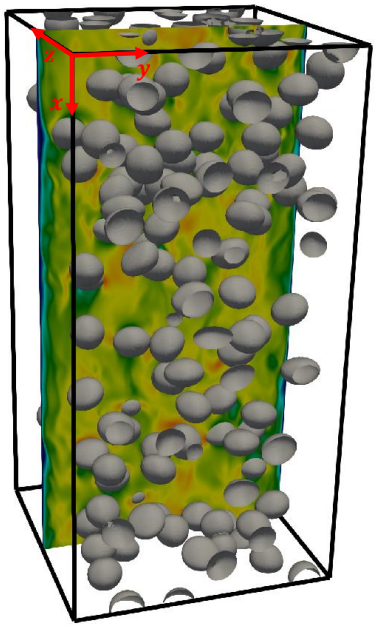

Figure 1: Volume fraction isosurfaces (grey, $\overline{f} = 0.5$) together with a wall-normal slice of the velocity magnitude on the mid-plane.

Both the density ratio ρ_l/ρ_g and the dynamic viscosity ratio μ_l/μ_g have been set to 20. The setup is investigated at a technically relevant gas fraction of 10%, which is achieved by inserting 195 initially spherical bubbles with an identical diameter of $d_b = 0.25H$. The chosen gravitational acceleration results in a Galilei number $Ga = \rho_l\sqrt{g d_b} d_b/\mu_l$ of $Ga = 417.1930$. Furthermore, the surface tension coefficient σ is such that the Eötvös number $Eo = \left(\rho_l g d_b^2\right)/\sigma$ is $Eo = 0.6667$. The combination of Eo and the bubble Reynolds number $Re_b = (\langle u_x\rangle_l - \langle u_x\rangle_g) d_b/\nu_l \approx 475$, which is based on the relative axial velocity of both phases, results in nearly spherical, mildly wobbling bubbles, as can also be seen in Figure 1.

All LES setups in this study are computed using $208 \times 104 \times 104$ uniform cubic cells, such that the bubbles are resolved with approximately 13 cells per diameter. To perform a first assessment of the SGS models, the LES results are compared to the results of a DNS of the same setup, which is conducted using twice the LES resolution (i.e., $416 \times 208 \times 208$ cubic cells, or approximately 26 cells per bubble diameter). Although this resolution does not fulfill the typical criteria for a DNS (i.e., resolution of the Kolmogorov length scale) and is slightly under-resolved, it already allows an initial consistency check regarding the trends arising for different models, as well as their interplay with the numerical scheme. The time step is controlled by setting $CFL = 0.2$, and all statistical quantities are averaged in space and time for several hundred flow-through times after reaching a statistically steady state.

5 Results

In order to assess the performance of different SGS models, this section compares the volume fraction and velocity statistics resulting from LES to those of the more detailed simulation. For brevity, the latter is referred to as DNS in this section, despite the shortcomings discussed above. All velocity statistics are normalized using the wall friction velocity $u_\tau = \sqrt{\tau_w/\rho_l}$ of the more detailed simulation. In the following, $\langle\cdot\rangle$ refers to averaging over the time, as well as the homogeneous directions x and z, which results in wall-normal profiles of the averaged quantities. The statistics are evaluated for the entire flow field, i.e., they are not conditioned on either the liquid or the gas phase. Due to the symmetry of the setup, the profiles have been averaged over both channel halves, and they are shown over the dimensionless wall distance $y^+ = y(u_\tau/\nu)$. For better clarity, the tilde denoting implicit filtering is omitted in the following.

Figure 2 shows the wall-normal profile of the average gas volume fraction. The DNS reveals similar results as known from previous work (e.g. Bräuer et al. 2021). Compared to the DNS results, the bubble-free zone near the wall is wider for the Smagorinsky model, while it is narrower for the SST models and the sensor-based modification of the Smagorinsky model. The profile for the sigma model matches the DNS profile relatively well up to $y^+ \approx 70$ and starts to deviate slightly afterwards. It overestimates the peak of the

gas fraction profile at $y^+ \approx 200$, just as the Smagorinsky model. The SST models and the sensor model match the peak relatively well, however it is located slightly too close to the walls. Since, compared to the DNS and the other models, the bubbles on average move closer to the walls for the latter ones, they reveal a weaker accumulation of bubbles in the channel center. In this region, the Smagorinsky and sigma model are closer to the DNS reference. The profile for the LES without an explicit SGS model overlaps with those of the SST-models and the sensor-based model for all values of y^+.

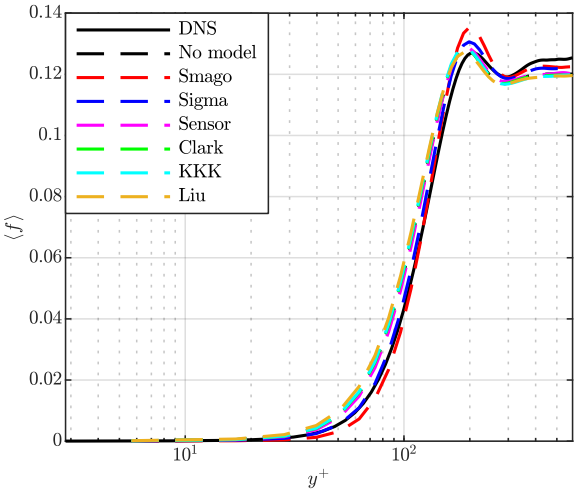

Figure 2: Average gas volume fraction $\langle f \rangle$ as a function of the dimensionless wall distance y^+.

The average stream-wise velocity profiles, normalized with u_τ of the DNS to yield the dimensionless velocity $\langle u^+ \rangle$, are presented in Figure 3. It is immediately apparent that the choice of an SGS model for momentum advection strongly influences the mean volumetric flow rate in axial direction. The DNS reveals the highest average stream-wise velocity. Of all LES models, the sigma model provides the best prediction for this quantity, followed by the sensor model. The latter leads to a slight improvement compared to the LES without SGS model, and to a significant improvement compared to the baseline Smagorinsky model, which again yields the worst results. Out of the three SST models, Clark's model reveals the best performance with respect to the stream-wise velocity, followed by Liu's scale-similarity model and the KKK-regularization of Clark's model. In this context, it is worth noting that the KKK-regularization mainly aims to stabilize SST models, which, without regularization, often lead to unstable simulations. However, presumably mostly due to the comparably dissipative nature of the QUICK scheme, Clark's model remains stable for the simulated setup.

Despite the significant deviations between the axial flow rates that are apparent from Figure 3, the bubble Reynolds number, which depends on the relative velocity between the bubbles and the surrounding liquid, only varies between $Re_b \approx 476.8$ for the DNS and $Re_b \approx 466.0$ for the LES with the Smagorinsky model. It can therefore be concluded that the comparison between DNS and LES remains meaningful in terms of the problem-characterizing dimensionless numbers.

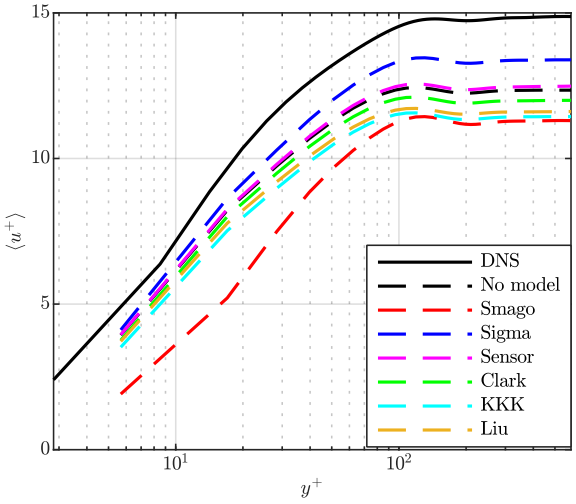

Figure 3: Average stream-wise velocity, normalized by the wall friction velocity u_τ to yield $\langle u^+ \rangle$, as a function of the dimensionless wall distance y^+.

Figures 4 to 6 show the root mean square (RMS) of the stream-wise, the wall-normal and the span-wise velocity fluctuations. As Figure 4 demonstrates, all LES profiles, apart from the one for the Smagorinsky model, correctly predict the location of the first peak of the stream-wise velocity fluctuations u', considering the low mesh resolution close to the wall. Once again, the sigma model overall leads to the best agreement between LES and DNS, especially in the near-wall region, but also for the second increase of the fluctuations towards the channel center. The sensor model once more slightly outperforms the LES without SGS model, and properly corrects the behavior of the Smagorinsky model. The SST models overall behave similarly to each other, irrespective of y^+. Directly in the channel core, there is hardly any difference between the DNS and the different LES profiles.

The deviation between the stream-wise fluctuation profiles is relatively large close to the walls, where the flow is dominated by wall turbulence, whereas it nearly vanishes for the mainly bubble-induced turbulence in the center of the channel. Since the differences in the near-wall behavior of u' qualitatively resemble the differences in the average stream-wise velocities (see Figure 3), it seems that the mean axial velocity is the main influencing factor close to the walls. In the channel center, however, all profiles quasi overlap, which might be indicative that the relative axial velocity of both phases, which also defines the bubble Reynolds number (see discussion above), is the decisive parameter for the fluctuation level.

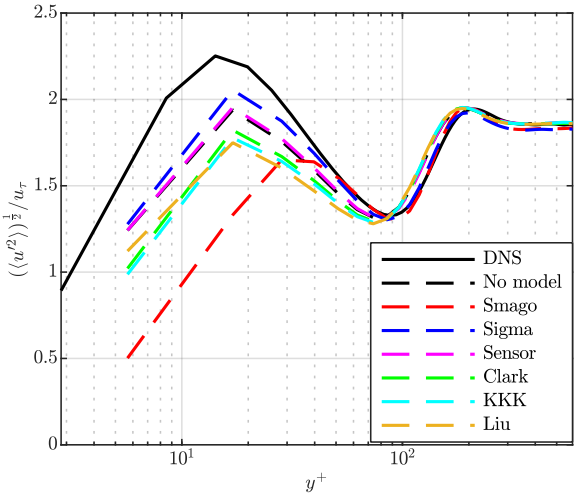

Figure 4: RMS of the stream-wise velocity fluctuations u', normalized by the wall friction velocity u_τ, as a function of the dimensionless wall distance y^+.

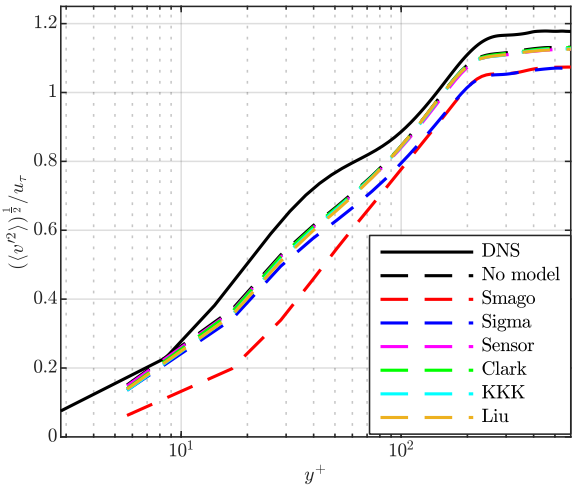

Figure 5: RMS of the wall-normal velocity fluctuations v', normalized by the wall friction velocity u_τ, as a function of the dimensionless wall distance y^+.

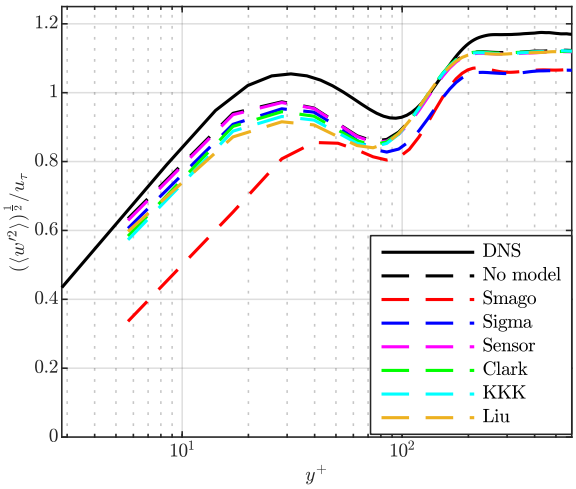

Figure 6: RMS of the span-wise velocity fluctuations w', normalized by the wall friction velocity u_τ, as a function of the dimensionless wall distance y^+.

The wall-normal velocity fluctuations are shown in Figure 5. Irrespective of y^+, the DNS shows the highest fluctuations, while the Smagorinsky model predicts the lowest fluctuations. Compared to the Smagorinsky model, the sigma model matches the DNS significantly better close to the walls, where it produces essentially the same results as the SST models, the sensor model, and the LES without model. However, with increasing distance to the wall, the sigma model deviates from the latter profiles, and approaches the one of the Smagorinsky model. The results for the SST models, the sensor model, and the LES without model are quasi indistinguishable for all values of y^+. The fact that this is not the case for the near-wall region of the stream-wise velocity fluctuations (see Figure 4) once again suggests that the differences in the stream-wise fluctuations are closely related to the difference in the axial flow rate. Overall, the SST models, the sensor model and the LES without SGS model reveal a better performance than the Smagorinsky and sigma model in terms of the wall-normal velocity fluctuations.

Figure 6 presents the span-wise velocity fluctuations. Overall, the results are similar to the wall-normal velocity fluctuations (see Figure 5). Apart from a short section at $y^+ \approx 150$, the highest fluctuations can be observed for the DNS, while the Smagorinsky model significantly underpredicts w'. The results for the LES without an explicit SGS model once again reveals nearly identical results to the LES using the sensor model. Also, both profiles are similar to those for the SST models. As previously discussed for the wall-normal velocity fluctuations, the sigma model behaves similarly to the SST models close to the wall, and continuously approaches the profile of the Smagorinsky model with increasing wall distance. With respect to the span-wise velocity fluctuations, the best results are obtained for the sensor model and the LES without an SGS model.

6 Conclusion and outlook

As *a-posteriori* analysis has shown, the volumetric flow rate in main flow direction depends strongly on the mesh resolution and the SGS model for momentum advection. Despite the significant deviations in the stream-wise flow velocity, the bubble Reynolds number remains largely unaffected, since the relative axial velocity between the gas and liquid phase is nearly identical for all LES setups and the DNS.

Across all investigated volume fraction and velocity statistics, the static Smagorinsky model produces the worst results. The sigma model, on the one hand, provides the best estimation for the average stream-wise velocity (and therefore for the average flow rate) and its fluctuation. On the other hand, it underestimates the wall-normal and span-wise velocity fluctuations in the channel center. The results for the sensor model are nearly identical to the results for the LES

without an explicit SGS model. Still, the sensor model leads to a slight improvement in terms of the axial velocity. Given its definition, the sensor model's behavior suggests that it almost permanently deactivates the SGS dissipation of the Smagorinsky model. The results revealed that the sensor model features a considerably lower mean turbulent viscosity compared to the Sigma model for this configuration. By increasing the constant C_{sensor} in such a manner that the mean subgrid scale dissipations coincide with each other, the differences between both models nearly vanish.

The three SST models, namely Clark's model, its regularization using the KKK-approach, as well as the scale similarity model by Liu, also behave very similarly to each other. Out of the three, Clark's model on average is closest to the DNS results in terms of the axial velocity and its fluctuation, while all other statistics do not allow further conclusions. For the given setup, it is evident that the investigated SST models do not lead to a clear improvement compared to the LES without an explicit SGS model.

When comparing the results across all investigated gas fraction and velocity statistics, the sigma model and the sensor-based modification of the Smagorinsky model on average reveal the best behavior. However, the results presented in this paper clearly highlight the challenges related to the modeling of the convective SGS contribution in the two-phase flow context. One particular aspect in this regard is the choice of the numerical scheme for momentum advection. On the one hand, central differencing schemes (CDS) are considered the best choices for the evaluation of models for the convective SGS term. However, in the two-phase flow context, using CDS can lead to unphysical oscillations or unstable simulations due to the singular surface tension force as well as the density and viscosity jumps at the interface. Using a more dissipative scheme, such as the QUICK scheme selected for this work, often resolves stability problems (Ketterl et al., 2019). In the context of *a-posteriori* assessment of SGS closures, however, using comparably dissipative schemes comes with clear disadvantages. Firstly, it is hardly possible to distinguish the dissipation intentionally introduced by the SGS model from the significant dissipation provided by the convection scheme. Secondly, more advanced modeling strategies, such as the KKK-regularization as well as the sensor-based Smagorinsky modification, are often deprived of their main advantages. This becomes clearly evident by, for example, comparing the results for the LES without SGS model to those for the sensor-based modification of the Smagorinsky model: due to the dissipative nature of the QUICK scheme, the model does not seem to considerably influence the simulation.

Consequently, to allow a more precise estimation of the model behavior, the next step will be to repeat the analysis using a CDS scheme. This will also include the validation of the LES results against a properly resolved DNS reference solution. For future work, it is also planned to increase the Eötvös number, which will lead to more deformable, oscillating bubbles. In this context, also an evaluation of SGS closures for the unresolved surface tension force is intended.

Acknowledgments

Support by the German Research Foundation (Deutsche Forschungsgemeinschaft - DFG, GS: KL1456/4-1) is gratefully acknowledged.

References

Anderson, B. & Domaradzki, J. (2012), A subgrid-scale model for large-eddy simulation based on the physics of interscale energy transfer in turbulence, *Physics of Fluids*, 24, 065104

Bräuer, F., Trautner, E., Hasslberger, J., Cifani, P. & Klein, M. (2021), Turbulent Bubble-Laden Channel Flow of Power-Law Fluids: A Direct Numerical Simulation Study, *Fluids*, 6, 40

Cifani, P., Kuerten, J & Geurts, B. (2018), Highly scalable DNS solver for turbulent bubble-laden channel flow, *Computers & Fluids*, 172, 67-83

Cifani, P. (2019), Analysis of a constant-coefficient pressure equation method for fast computations of two-phase flows at high density ratios, *Journal of Computational Physics*, 398, 108904

Clark, R., Ferziger, J. and Reynolds, W. (1979), Evaluation of subgrid-scale models using an accurately simulated turbulent flow, *Journal of Fluid Mechanics*, 91, 1-16

Coyajee, E. & Boersma, B. (2009), Numerical simulation of drop impact on a liquid-liquid interface with a multiple marker front-capturing method, *Journal of Computational Physics*, 228, 4444-4467

Dodd, M. & Ferrante, A. (2014), A fast pressure-correction method for incompressible two-fluid flows. *Journal of Computational Physics*, 273, 416-434

Hasslberger, J., Engelmann, L., Kempf, A. & Klein, M. (2021), Robust dynamic adaption of the Smagorinsky model based on a sub-grid activity sensor, *Physics of Fluids*, 33, 015117

Ketterl, S., Reissmann, M. & Klein, M. (2019) Large eddy simulation of multiphase flows using the volume of fluid method: Part 2 - A posteriori analysis of liquid jet atomization, *Experimental and Computational Multiphase Flow*, 1(3), 201-211

Klein, M., Ketterl, S. & Hasslberger, J. (2019), Large eddy simulation of multiphase flows using the volume of fluid method: Part 1 - Governing equations and a priori analysis, *Experimental and Computational Multiphase Flow*, 1(2), 130-144

Klein, M., Ketterl, S., Engelmann, L., Kempf, A. & Kobayashi, H. (2020), Regularized, parameter free scale similarity type models for Large Eddy Simulation, *International Journal of Heat and Fluid Flow*, 81, 108496

Liu, S., Meneveau, C. & Katz, J. (1994), On the properties of similarity subgrid-scale models as deduced from measurements in a turbulent jet, *Journal of Fluid Mechanics*, 275, 83-119

Nicoud, F., Toda, H., Cabrit, O., Bose, S. & Lee, J. (2011), Using singular values to build a subgrid-scale model for large eddy simulations, *Physics of Fluids*, 23, 085106